ChemPubSoc Europe

DOI: 10.1002/chem.201304240

CHEMISTRY
A European Journal
Full Paper

Enantioselectivity

Mukaiyama–Michael Reactions with *Trans*-2,5-Diarylpyrrolidine Catalysts: Enantioselectivity Arises from Attractive Noncovalent Interactions, Not from Steric Hindrance

Eeva K. Kemppainen,[a] Gokarneswar Sahoo,[a] Antti Piisola,[a] Andrea Hamza,[b] Bianka Kótai,[b] Imre Pápai,*[b] and Petri M. Pihko*[a]

Abstract: The scope of the enantioselective Mukaiyama–Michael reactions catalyzed by *trans*-2,5-diphenylpyrrolidine has been expanded to include both α- and β-substituted enals. However, the rationalization of the observed enantioselectivity is far from obvious since the catalyst is not very sterically hindered. DFT calculations were carried out to rationalize the observed stereoselectivities. Transition states of the C–C bond formation between iminium intermediates and silyloxyfurans were located and their relative energies were used to estimate the stereoselectivity data. We find excellent agreement between the predicted and observed stereoselectivities. The analysis of intermolecular forces reveals that the enantioselectivity is mostly due to stabilizing noncovalent interactions between the reacting partners, not due to steric hindrance. The role of attractive noncovalent interactions in enantioselective catalysis may be underappreciated.

Introduction

In enantioselective catalysis with organocatalysts or metal complexes, a typical rationalization for the observed enantioselectivity arises from steric hindrance present in alternative diastereomeric transition states leading to the enantiomer of the product.[1] These rationalizations are frequently used in metal catalysis[2] as well as in covalent organocatalysis.[3] Models based on steric hindrance are highly useful as they often allow the prediction of enantioselectivity for new substrates through empirically derived "enantioselectivity mnemonics".[4] Steric parameters can even be used in a systematic optimization of catalyst performance.[5] In enamine and iminium catalysis, models based on sterics have been highly successful in predicting the sense of enantioselectivity of a wide variety of transformations.[3] It is, however, important to bear in mind that synthetically useful enantioselectivities could equally well arise from attractive, not repulsive interactions, even in covalent catalysis. Herein, we present the case of a covalent iminium-catalyzed reaction in which the selectivity cannot readily be rationalized on the basis of sterics.

In conjunction with our research program towards the total synthesis of pectenotoxin-2,[6] we recently needed a method that would allow us to introduce a tertiary stereogenic center at C25 and a methyl group stereoselectively at C27 (Scheme 1).

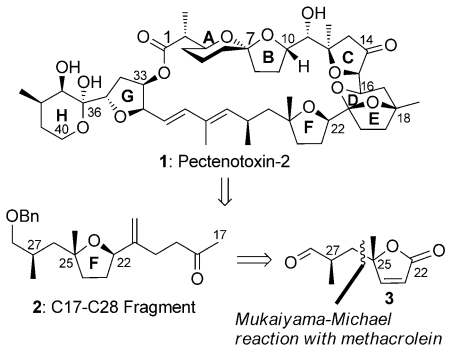

Scheme 1. Pectenotoxin (**1**) and the F-ring fragment (**2**).

We anticipated that a simple method for accessing this stereochemistry would involve an enantioselective Mukaiyama–Michael reaction between a silyloxyfuran **13** and enal **14** (Table 1). As described in our initial communication,[7] iminium-catalyzed reactions with α-substituted enals are rare, and reactions proceeding with a high enantioselectivity typically require a cyclization step.[8] However, we found, to our surprise, that α-substituted enals can readily be engaged in Mukaiyama–Michael reactions with high enantioselectivity by using

[a] *Dr. E. K. Kemppainen, Dr. G. Sahoo, A. Piisola, Prof. P. M. Pihko*
Department of Chemistry,
University of Jyväskylä, P. O. Box 35
40014, University of Jyväskylä (Finland)
E-mail: petri.pihko@jyu.fi

[b] *A. Hamza, B. Kótai, Dr. I. Pápai*
Research Centre for Natural Sciences
Hungarian Academy of Sciences
Pusztaszeri ut 59-67, H-1025, Budapest (Hungary)
E-mail: papai.imre@ttk.mta.hu

Supporting information for this article is available on the WWW under http://dx.doi.org/10.1002/chem.201304240.

trans-2,5-diphenylpyrrolidine as the catalyst.[9] In the following, we present a full account of these studies, including an expanded scope of the Mukaiyama–Michael reaction and a computationally derived rationalization for the observed enantioselectivity.

Results and Discussion

Catalyst screen

The initial catalyst screen of the Mukaiyama–Michael reaction between methacrolein (**14**) and 5-Me-silyloxyfuran **13** consisted of two well-established catalyst families (Table 1); the MacMillan catalysts[10] and various diarylprolinol derivatives (Jørgensen- and Hayashi-type catalysts).[11] However, the enantioselectivies obtained with these catalysts were suboptimal and prompted us to investigate other options for this transformation. We discovered that *trans*-2,5-diphenylpyrrolidine (**12**) performed far better in the reaction than any of the other tested catalysts.

Table 1. Catalyst screen for the Mukaiyama–Michael reaction.

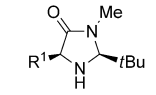

4: R^1=Bn
5: R^1=H

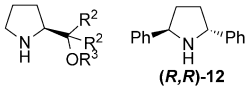

6: R^2 = 3,5-$(F_3C)_2C_6H_3$, R^3 = $SiMe_3$
7: R^2 = Ph, R^3 = $SiMe_3$
8: R^2 = Ph, R^3 = $SiPh_2Me$
9: R^2 = 3,5-$(F_3C)_2C_6H_3$, R^3 = $SiPh_2Me$
10: R^2 = 2-naphthyl, R^3 = $SiPh_2Me$
11: R^2 = 2-naphthyl, R^3 = $SiMe_3$

(*R*,*R*)-**12**

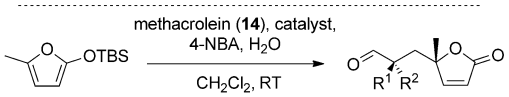

13

15a: R^1 = H, R^2 = Me
15b: R^1 = Me, R^2 = H

Entry	Catalyst	Conv. [%][a]	e.r.[b] (**15a/b**)	d.r.[b] (**15a/b**)
1	**4**	33	49:51/51:49	55/45
2	**5**	>95	68:32/61:39	64/36
3	**6**	65	60:40/64:36	65/35
4	**7**	94	77:23/76:24	57/43
5	**8**	>95	80:20/81:19	56/44
6	**9**	>95	64:36/82:18	59/41
7	**10**	>95	79:21/80:20	56/44
8	**11**	76	65:35/69:31	58/42
9	(*R*,*R*)-**12**	>95	3:97/4:96[c]	56/44

[a] Determined by GC, monitoring the conversion of silyloxyfuran **13** to **15a/15b** during the reaction. [b] Determined by GC (Supelco® Astec® CHIRALDEX® B-DM column). [c] Designates the opposite enantiomers of **15a/15b**. NBA = nitrobenzoic acid.

Optimization of the reaction conditions

The initial conditions used for the catalyst screening were adapted from those used by MacMillan and co-workers. However, it was not evident that these conditions (biphasic mixture of CH_2Cl_2/H_2O, 4-nitrobenzoic acid co-catalyst) would be optimal for the reactions with catalyst **12**, and additional optimization was warranted. Initially, the plan was to monitor the reactions by using online ^{1}H NMR spectroscopic monitoring, but this plan was abandoned due to very slow progress of the reaction in the NMR tube. For the reactions to proceed, rapid stirring of the reaction is necessary.

During the catalyst screening, it was observed that TMS-protected silyloxyfurans were labile under our aqueous reaction conditions and the silyloxyfuran **16** was rapidly hydrolyzed to the starting lactone. Additionally, control experiments indicated that the TMS-protected silyloxyfuran could undergo the Mukaiyama–Michael reaction directly under acid catalysis, leading to a racemic product and thus reduced enantioselectivity. In contrast, *t*-butyldimethylsilyl (TBS)- and triisopropylsilyl (TIPS)-protected silyloxyfurans (**13** and **17**) were less prone to (though not immune to) these side reactions and therefore these silyloxyfurans were selected for the further studies (Table 2).

Table 2. Effect of the silyl group on the enantioselectivity.

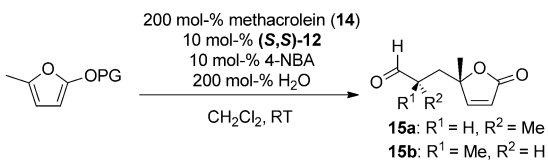

15a: R^1 = H, R^2 = Me
15b: R^1 = Me, R^2 = H

Entry	PG	*t* [h]	e.r.[a]	d.r.[b] (**15a/b**)	Yield [%][a]
1	TMS (**16**)	<3	90:10	55:45	<10
2	TBS (**13**)	8	97:3	58:42	>95
3	TIPS (**17**)	24[c]	97:3	58:42	>95

[a] Determined by GC (Supelco® Astec® CHIRALDEX® B-DM column) from the reaction mixture. In general, the enantiomeric ratio (e.r.) was similar (±2%) for both diastereomers. [b] Determined by GC (Supelco® Astec® CHIRALDEX® B-DM column) from the reaction mixture. [c] The reaction was likely completed earlier but it was not monitored continuously.

Screening of the acid co-catalyst revealed that the stronger acids led to more prominent and faster side reactions (Table 3). The lipophilicity of the acid also played a role, as both strongly hydrophilic and lipophilic acids significantly slowed the reaction rate. In our reaction conditions, the moderately lipophilic 4-nitrobenzoic acid was the optimal choice.

The use of 200 mol% of the α-substituted acroleins (**14**, **25**–**28**) was sufficient to consume all the silyloxyfuran starting material. However, when acrolein (**18**) was used as the substrate, it was observed that the reaction did not go to completion. Additionally, the rate of product formation slowed drastically when the concentration of acrolein diminished, and the highest concentration of product (55% yield) was reached only after 23 h with 20 mol% of catalyst, and after 52 h with 10 mol% of catalyst. Using a larger excess of acrolein (up to 1000 mol%, versus the 200 mol% used previously) dramatically increased both the highest concentration of product as well as

Table 3. Screening of the acid co-catalysts for the Mukaiyama–Michael reaction.

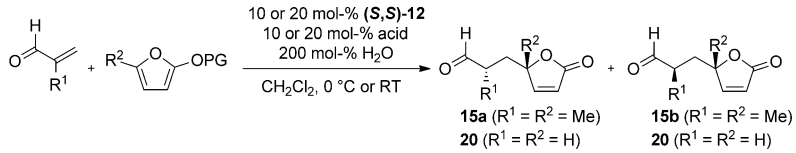

Entry[a]	R^1	R^2	PG	Acid	pK_a[b]	logP[b]	*t* [h]	Yield [%][c]	e.r.[c]	d.r.[d]
1	Me (**14**)	Me	TBS (**13**)	TFA	0.05	1.35	2	63	93:7	57:43
2	Me (**14**)	Me	TBS (**13**)	2-NBA	2.19	1.19	5	75	97:3	56:44
3	Me (**14**)	Me	TBS (**13**)	3-NBA	3.48	1.68	4	81	96:4	56:44
4	Me (**14**)	Me	TBS (**13**)	$ClCH_2COOH$	2.65	0.05	21	>95	94:6	56:44
5	Me (**14**)	Me	TBS (**13**)	4-NBA	3.42	1.79	8	>95	97:3	55:45
6	Me (**14**)	Me	TBS (**13**)	Formic acid	3.74	−0.54	21	>95	96:4	57:43
7	H (**18**)	H	TIPS (**19**)	2,4-DNBA	1.43	1.34	2	37	94:6	–
8	H (**18**)	H	TIPS (**19**)	3,5-DNBA	2.77	1.71	2	40	89:11	–
9	H (**18**)	H	TIPS (**19**)	4-NBA	3.44	1.79	1	70[d]	95:5	–
10	H (**18**)	H	TIPS (**19**)	3,5-dichlorobenzoic acid	3.46	3.50	4	60	94:6	–
11	H (**18**)	H	TIPS (**19**)	Lactic acid	3.91	−0.85	2	45	89:11	-

[a] For entries 1–6, 10 mol% of catalyst and acid were used and the reactions were run at RT. For entries 7–11, 20 mol% of catalyst and acid were used and the reactions were run at 0 °C. [b] The values are taken from SciFinder (http://scifinder.cas.org), and are reportedly generated by using Advanced Chemistry Development (ACD/Labs) Software V11.02 (© 1994–2013 ACD/Labs). [c] Determined by using GC (Supelco® Astec® CHIRALDEX® B-DM column) from the reaction mixture. [d] Determined by using NMR spectroscopy from the reaction mixture. In general, the enantiomeric ratio (e.r.) was similar (±2%) for both diastereomers. TFA = trifluoroacetic acid, DNBA = dinitrobenzoic acid.

problems were not observed with the 5-methyl-substituted butenolide products.

Variation of the aryl ring of the catalyst (Table 4) revealed that the original *trans*-2,5-diphenylpyrrolidine catalyst was nearly optimal. Interestingly, catalysts **21** and **24** bearing alkyl substituents in the aromatic ring were obtained at suboptimal enantiomeric purity, which of course further lowers the observed enantioselectivities. Nonetheless, no improvement in selectivity from substitutions in the aryl ring is apparent.

Substrate scope with substituted acroleins

In addition to methacrolein, various α-substituted acroleins[12] were studied in the Mukaiyama–Michael reaction. The α-acroleins were subjected to the optimized Mukaiyama–Michael reaction conditions with TBS- or TIPS-protected silyloxyfurans (Table 5).

The screens revealed that the reaction tolerates both α-alkyl and α-oxy-substituted aldehydes (Table 5, entries 4–7 and 8–10, respectively). Methacrolein appears to be the most optimal substrate, furnishing the isolated product in 90% yield with excellent enantioselectivity by using only 10 mol% of the catalyst **12** and TBS-protected furan **13** (Table 5, entry 5). In other entries, 20 mol% of the catalyst was used with TIPS-protected silyloxyfurans, affording the isolated product in 60–70% yields with good-to-excellent enantioselectivities. Two exceptions to the high enantioselectivities can be noted in Table 5: Entry 3, in which the silyloxyfuran **29** bears a C3-methyl substituent, and entry 7, in which α-benzylacrolein **26** was used. With **26**, the lower selectivity of the reaction may be related to the sluggishness of the reaction. The explanation for the lower selectivity obtained with **29** (Table 5, entry 3) will be discussed below.

In general, stereocontrol of the aldehyde α-substituent was not possible due to rapid equilibration, and the products were obtained in ratios ranging from 1:1 to 2:1. However, in many cases, the diastereomers are readily separable by chromatography, and equilibration of the product diastereomers is also possible, allowing the steering of the product composition to either diastereomeric direction.[7]

In addition to α-substituted acroleins, catalyst **12** also gave excellent enantioselectivities in reactions with β-substituted acroleins (Table 6), albeit with moderate-to-good diastereoselectivities. The diastereomeric ratio is particularly encouraging for the R^2 = Me and R^3 = Me combination (Table 6, entries 1 and 2, respectively), but they become deteriorated for unsubstituted silyloxyfurans (entries 3 and 4, respectively).

the reaction rate (70% yield reached after only one hour). In summary, using a large excess of acrolein was crucial to the success of the reaction.

It was also observed that products with a proton in the 5-position of the furan-2-one ring were prone to slowly decompose under the reaction conditions, leading to low yields if the reactions were left to proceed for several days. However, these

Table 4. Screening of catalysts for the Mukaiyama–Michael reaction.

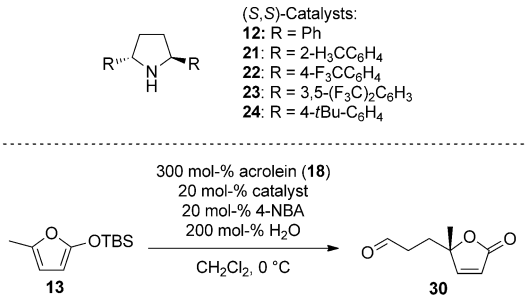

Entry	Catalyst (e.r. of catalyst)	e.r. of product[a]
1	**12** (98:2)	97:3
2	**21** (85:15)	78:22
3	**22** (99:1)	94:6
4	**23** (98:2)	93:7
5	**24** (95:5)	87:13

[a] Determined by using GC (Supelco® Astec® CHIRALDEX® B-DM column) from the reaction mixture.

Table 5. Substrate scope for α-substituted acroleins.

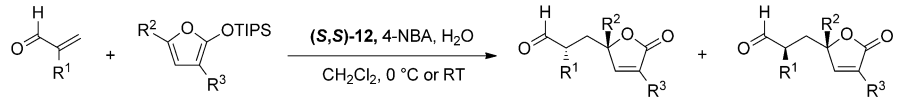

Entry	R^1	R^2	R^3	Yield [%]	T [°C]	e.r.[a]	d.r. [(*S*,*S*)/(*R*,*S*)]	Product
1	H (**18**)	H	H (**19**)	61	0	94:6	–	**20**
2	H (**18**)	Me	H (**17**)	65	0	96:4	–	**30**
3	H (**18**)	H	Me (**29**)	40	0	85:15	–	**31**
4	Me (**14**)	H	H (**19**)	53	0	98:2	50:50	**32**
5	Me (**14**)	Me	H (**13**)[b]	90	0	98:2	55:45	**15**
6	*n*-Pr (**25**)	Me	H (**17**)	58	0	95:5	57:43	**33**
7	Bn (**26**)	Me	H (**17**)	69	RT	85:15[c]	48:52	**34**
8	AcO (**27**)	H	H (**19**)	58	0	97:3[d]	64:36	**35**
9	AcO (**27**)	Me	H (**17**)	71	RT	97:3[e]	50:50	**36**
10	BnO (**28**)	Me	H (**17**)	61	RT	98:2	63:37	**37**

[a] Determined by using GC (Supelco® Astec® CHIRALDEX® B-DM column). In general, the enantiomeric ratio (e.r.) was similar (±2%) for both diastereomers. [b] TBS-protected silyloxyfuran was used. [c] Determined by using HPLC (Chiralcel® IC column) from the alcohol derivative. [d] Determined by using HPLC (Chiralcel® IC column) from the 5,5-dimethyl-1,3-dioxan-2-yl-derivative. [e] Determined by using HPLC (Chiralcel® IB column) from the 5,5-dimethyl-1,3-dioxan-2-yl-derivative.

Table 6. Substrate scope for β-substituted acroleins.

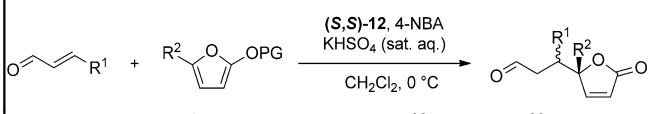

Entry	R^1	R^2	PG	Yield [%][c]	e.r.[a]	d.r.[a]	Product
1	Me (**38**)	Me	TBS (**13**)	52	96:4	94:6	**41**
2	Me (**38**)	Me	TIPS (**17**)	64	97:3	91:9	**41**
3	Me (**38**)	H	TBS (**40**)	57	95:5/98:2[b]	58:42	**42**
4	Me (**38**)	H	TIPS (**19**)	56	95:5/96:4[b]	49:51	**42**
5	*n*-Pr (**39**)	Me	TIPS (**17**)	64	93:7/97:3[b]	81:19	**43**
6	*n*-Pr (**39**)	H	TIPS (**19**)	70	98:2/93:7[b]	77:23	**44**

[a] Determined by using GC (Supelco® Astec® CHIRALDEX® B-DM column) from the reaction mixture. [b] e.r. reported for both diastereomers. [c] Isolated yields.

Rationalization of the enantioselectivity

To gain an insight into the origin of stereoselectivity of the present Mukaiyama–Michael transformations, some of the observed reactions were examined computationally. We primarily focus on the reaction between methacrolein (**14**) and TBS-protected 5-Me-silyloxyfuran **13** (Table 5, entry 5), but results for reactions with acrolein and (*E*)-crotonaldehyde are also discussed. It is assumed herein that the reactions follow the classical iminium-catalyzed pathway[3a] and the C–C bond formation between the iminium intermediates and silyloxyfurans represents the stereoselectivity-determining step. Transition states corresponding to this elementary step were located and analyzed by using high-level DFT calculations. The relative energies of transition states leading to different stereoisomeric products were used to estimate the stereoselectivity data.[13]

Four different isomeric forms of the iminium species derived from methacrolein and catalyst **12** were identified computationally (see Figure 1). The most stable conformer corresponds to the *s-trans* arrangement of the conjugated double bonds and the envelope shape of the pyrrolidine ring (**im-*s-trans***). The half-chair ring-conformation of pyrrolidine (hereafter labelled by prime (′)) gives rise to another *s-trans* conformer (**im-*s-trans*′**), which lies only 0.5 kcal mol^{-1} higher in energy. The corresponding *s-cis* conformers (**im-*s-cis*** and **im-*s-cis*′**) are predicted to be slightly less stable, however, the conjugated π-system in these forms deviate significantly from the ideal planar structure (see dihedral angles in Figure 1). Such distortions imply reduced electrophilicitites of these species, which likely affects their reactivities towards silyloxyfurans.[14] Our calculations indicate that these iminium conformers can easily interconvert, therefore they are assumed to be in equilibrium in the reaction mixture. For TBS-protected 5-Me-silyloxyfuran, a number of close-lying conformers were found, differing in the position of the silyloxy arm and the orientation of the silyl group. These conformers are predicted to be nearly isoenergetic and the conversion barriers are found to be very small (≈1 kcal mol^{-1}).[15] Consequently, the bulky silyl groups of the silyloxyfurans do not necessarily impose steric hindrance upon the C–C bond-formation process, because the silyl group can readily rotate out of the way.

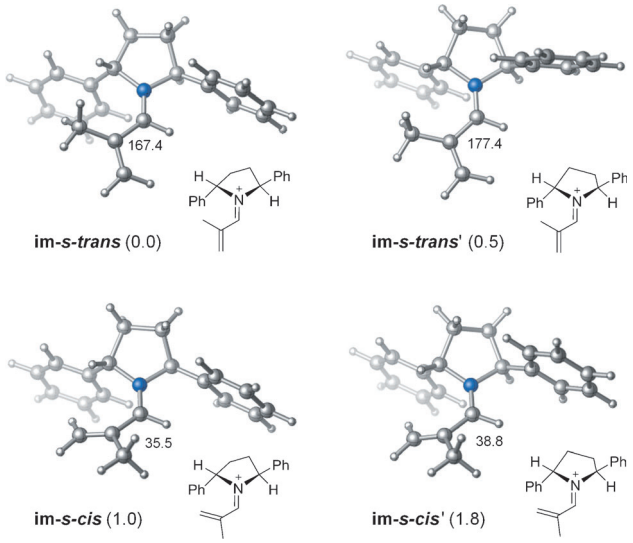

Figure 1. Conformers identified computationally for the iminium cation derived from methacrolein and catalyst **12**. Relative stabilities (in kcal mol^{-1}, with respect to the most stable structure) are shown in parenthesis. Dihedral angles defined by the atoms of the N=C–C=C unit are given in degrees.

The transition states were explored through an extensive conformational analysis. We find that closed transition structures, that is, those that display maximum contact between the iminium and furan π-systems, are clearly favored over the open structures.[15,16] In line with the reduced electrophilicities of the *s-cis*-type iminium isomers, the corresponding transition states are predicted to be notably less stable (by about 5 kcal mol^{-1}) than those originating from the *s-trans* iminium structures. Consequently, the *s-cis*-type transition states were excluded from our consideration.

Four different arrangements of the reacting iminium and silyloxyfuran species are possible that maximize the contact between the furan and iminium π-systems. These are illustrated in Figure 2. For instance, in transition state "d/*si*", the furan approaches the iminium π-system from below the iminium ion ("down" direction) with its *si* face. By using this notation, transition states "d/*si*" and "u/*si*" lead to *S* products, whereas "d/*re*" and "u/*re*" transition states give *R* products.

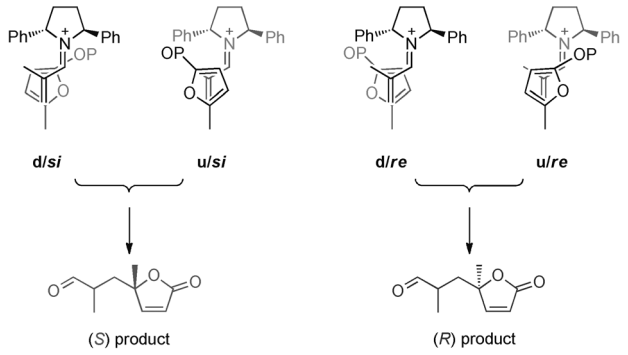

Figure 2. Labeling of transition states in the reaction of iminium and silyloxyfuran species. Labels "d" and "u" indicate the direction of the furan attack (down and up positions, respectively); "*si*" and "*re*" refer to the two faces of the furan molecule. P denotes the protecting TBS group. Note that due to two possible conformations of the pyrrolidine ring, the number of transition states is doubled.

Considering the two possible conformations of the pyrrolidine ring, eight low-lying C–C bond-formation transition states could be located for the reaction between methacrolein and TBS-protected 5-Me-silyloxyfuran. The relative energies of the transition states and their percentage contributions to the formation of *S* and *R* product isomers are given in Table 7.

It is apparent from these results that the silyloxyfuran attacks preferentially by its *si* face on the iminium intermediate. All combinations of *si*-type transition states lie lower in energy than the corresponding *re* analogues, therefore the formation of the *S*-product isomer is predicted to be favored kinetically. Structures **TS-d/*si*′** and **TS-u/*si*′** represent the most stable transition states leading to the major product, and they are both characterized by close intermolecular contacts between the bulky protecting group and the pyrrolidine/phenyl units of the catalyst (see Figure 3). These interactions are present in the most favored *re*-type transition states as well (**TS-u/*re*** and **TS-d/*re*′** in Figure 3), however, they are over 3 kcal mol^{-1} less stable than the *si*-type transition states. The enantiomeric ratio (e.r. (*S*/*R*)) computed from the relative energies of the full set of transition states is 99.7:0.3, which is in agreement with the experimental observations.

Table 7. Computed relative energies of transition states and related stereoselectivity data for the reaction of methacrolein and TBS-protected 5-Me-silyloxyfuran.

Notation[a]	Iminium	Attack	Product	ΔE [kcal mol^{-1}]	Pop [%][b]
TS-d/*si*	*s-trans*	d/*si*	*S*	2.29	1.2
TS-u/*si*	*s-trans*	u/*si*	*S*	1.52	4.2
TS-d/*re*	*s-trans*	d/*re*	*R*	5.34	0.0
TS-u/*re*	*s-trans*	u/*re*	*R*	3.33	0.2
TS-d/*si*′	*s-trans*′	d/*si*	*S*	0.00	56.2
TS-u/*si*′	*s-trans*′	u/*si*	*S*	0.23	38.1
TS-d/*re*′	*s-trans*′	d/*re*	*R*	3.77	0.1
TS-u/*re*′	*s-trans*′	u/*re*	*R*	4.87	0.0
e.r. (*S*/*R*)					99.7:0.3

[a] In the first four structures, the pyrrolidine has an envelope shape, and in the last four structures (labelled by prime) the pyrrolidine adopts a half-chair ring conformation. [b] The relative contributions of various pathways to the formation of product isomers are obtained from Maxwell–Boltzmann statistics: $pop_i = 100 \times \exp(-\Delta E_i/RT)/\Sigma_i[\exp(-\Delta E_i/RT)]$.

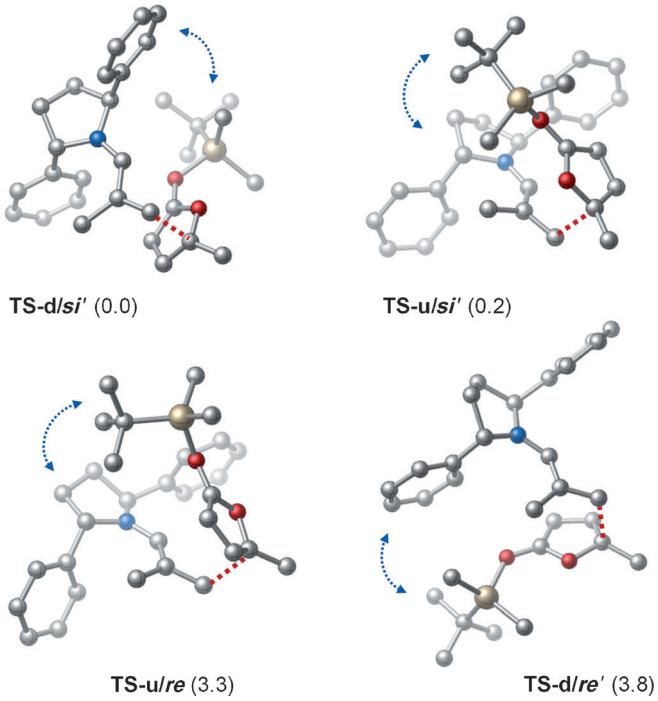

Figure 3. Structures of the most stable *si*- and *re*-type transition states. Relative stabilities (in kcal mol^{-1}, with respect to the most stable structure) are shown in parenthesis. The developing C–C bonds are indicated by the dashed lines; some of the intermolecular contacts are highlighted by arrows. All hydrogen atoms are omitted for clarity.

In iminium catalysis, the prevailing paradigm is that selectivity is controlled by steric effects.[3a] The importance of attractive secondary interactions has also been noted,[17] especially in controlling the conformation of the iminium cation.[18] Our structural analysis reveal relatively short intermolecular H···H distances (2.2–2.3 Å) in the transition states. These distances might point to certain degree of steric congestion. However,

an alternative explanation is that these contacts can give rise to stabilizing van der Waals interactions as well. To gain insight into the nature of these intermolecular forces, we generated reduced density gradient (RDG) isosurface plots for the transition states using the method developed by Yang et al.[19,20] This analysis allows one to identify and characterize regions of noncovalent interactions (NCI) in real space by locating low electron-density and low RDG domains in a molecular system. The NCI plot obtained for the most stable transition state (**TS-d/*si*′**) is depicted in Figure 4.

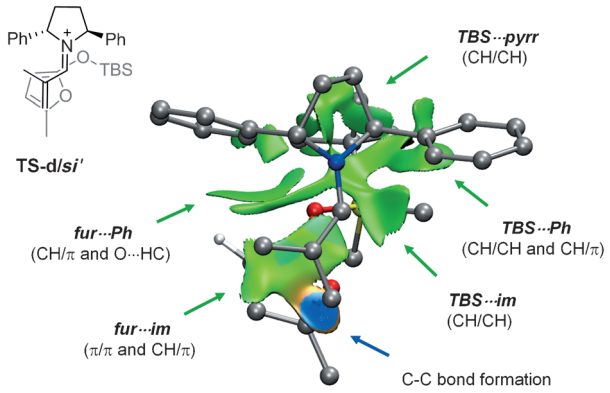

Figure 4. NCI plot generated for transition state **TS-d/*si*′**. Green regions represent weak noncovalent interactions; the blue region corresponds to C–C bond formation. Applied cutoff for the gradient is $s = 0.3$ au. Various fragments of reacting species are abbreviated as: *fur*: furan ring, *im*: N=C–C=C moiety of the iminium, *pyrr*: pyrrolidine ring. The specific types of interactions are shown in parenthesis.

The RDG isosurface plot displays broad contact areas between the reacting species. The green regions are indicative of weak and attractive noncovalent interactions, which can be classified according to the involved molecular units. For instance, favorable interactions between the iminium and furan π-systems are represented by a large surface area (*fur···im* in Figure 4). Interestingly, the furan ring and the silyloxy oxygen interact notably with the phenyl group of the catalyst (*fur···Ph*). As noted above, the alkyl groups of the TBS group interacts extensively with the pyrrolidine and Ph units of the catalyst, and these regions can also be clearly identified in the plot (*TBS···pyrr* and *TBS···Ph*). Finally, the methyl groups of the TBS group interact with the unsaturated iminium as well, as indicated by *TBS···im* interactions in Figure 4. All these specific contacts can be considered as weak intermolecular van der Waals interactions, providing stabilization for the transition states and directly affecting the stereoselectivity of the reaction.

The NCI plots of the most favored *si*- and *re*-type transition states are shown in Figure 5. Visual inspection of these plots suggest that some of the noncovalent interactions, such as *fur···im* and *TBS···im*, are always present in the transition states and therefore they are unlikely to play an important role in the stereocontrol. It is apparent that the other interactions (*TBS···pyrr*, *TBS···Ph* and *fur···Ph*) occur concurrently in *si*-type transition states, but this is not the case for the two *re*-type structures. In the transition state **TS-u/*re***, the furan ring is displaced far from the Ph group, so no *fur···Ph* interactions are observed, whereas in **TS-d/*re*′**, the TBS group interacts solely with the one of the Ph groups (and not with the pyrrolidine ring). It thus appears that the origin of stereoselectivity might be related to the unbalanced overall weight of these specific noncovalent interactions.

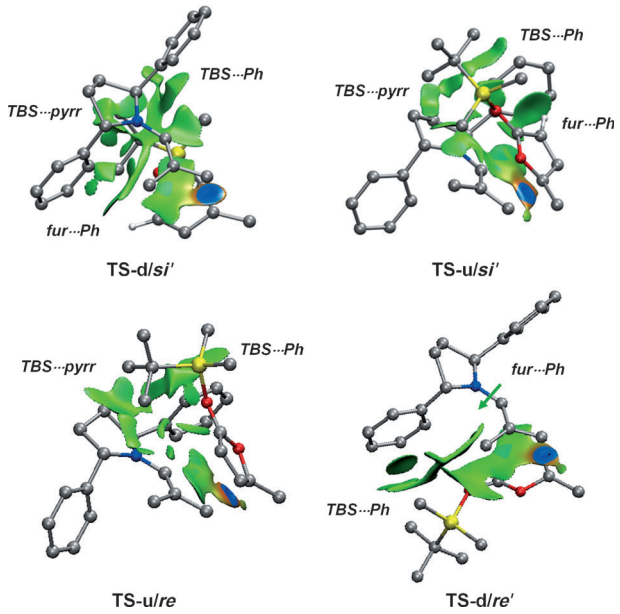

Figure 5. NCI plots for the most stable *si*- and *re*-type transition states. Characteristic van der Waals contacts are highlighted for each structure.

To quantify the contribution of *fur···Ph* and *TBS···Ph/pyrr* interactions to the transition-state stabilization, we constructed two truncated models as illustrated in Figure 6. In *model-1*, the TBS group of the silyloxyfuran is replaced by a SiH_3 group, whereas in *model-2*, the furan ring is omitted and the protecting group is represented by silane TBS–H. Interaction energies between the iminium intermediate and the truncated substrates were computed for geometries identical to the original transition states.[21] The results are reported in Table 8.

The interaction energies computed through *model-1* are fairly large because they incorporate attractive interactions between structurally distorted reactants.[22] The largest value is

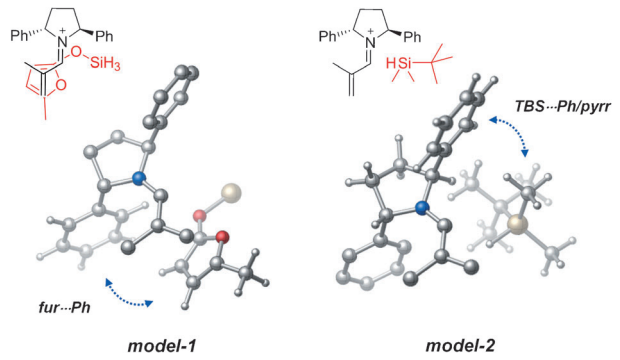

Figure 6. Truncated models of transition states (as exemplified by **TS-d/*si*′**) used to estimate the relative strength of *fur···Ph* and *TBS···Ph/pyrr* interactions. Hydrogen atoms not involved in specified interactions are omitted for clarity. Note that the *fur···Ph* interaction is of C–H···π type.

Table 8. Interaction energies obtained from computations on truncated models (see Figure 6).[a]

Notation	*Model-1*	*Model-2*	Sum[b]
TS-d/*si*′	−26.7	−10.2	−36.9
TS-u/*si*′	−30.1	−9.0	−39.1
TS-u/*re*	−24.8	−9.8	−34.6
TS-d/*re*′	−26.8	−7.9	−34.7

[a] Energies are reported in kcal mol^{-1}. [b] The sum of the two interaction energies.

predicted for **TS-u/*si*′**, which can be associated with enhanced *fur*···*Ph* interactions arising from a nearly optimal T-shape stacking arrangement of the two rings (see Figure 5). In comparison, this model gives a significantly reduced interaction energy for **TS-u/*re***, which is clearly due to the absence of the *fur*···*Ph* contact.[23] The results obtained by *model-2* point to notable stabilizing *TBS*···*Ph/pyrr* interactions, which range between 8–10 kcal mol^{-1}. However, the lack of *TBS*···*Ph* contacts in **TS-d/*re*′** result in reduced stabilization for this transition state. Although the stabilization effects predicted by the two models are not additive, the sum of the interaction energies is in qualitative agreement with the relative stabilities of the original transition states.

The prediction that *fur*···*Ph* interactions are important for selectivity can be tested. In both **TS-d/*si*′** and **TS-u/*si*′**, the H3 hydrogen of furan makes a close contact with the pi system of the phenyl ring. Indeed, a 3-methyl-substituted silyloxyfuran **29** (Table 5, entry 3) leads to significantly lower enantioselectivity, in agreement with the hypothesis that the *fur*···*Ph,* which may be largely a C–H···π-type interaction, is partially responsible for the high selectivity.

The overall picture that emerges from the computational studies is that high enantioselectivity can evolve from the interplay of attractive, not repulsive, intermolecular interactions. In this case, the favored orientation of the silyloxyfuran ring over the methacrolein-derived iminium ion enables the exploitation of the stabilizing noncovalent interactions between the reaction partners. Further support for this view is obtained from the analysis of the relative orientation of the *tert*-butyl and methyl groups of the TBS moiety in the transition states. As illustrated in Figure 7, the bulky *tert*-butyl group of the TBS prefers to orient towards, not away from, the pocket created by the pyrrolidine and the phenyl rings of the catalyst.

The C–C bond-formation transition states for the reaction of acrolein with silyloxyfuran **13** were also located and analyzed in our theoretical study and the results are presented in Table 9. Similarly to the previous reaction, the *si*-type transition states are systematically more stable than their *re* analogues leading to a very high enantiomeric ratio. The *si*-type transition states originating from *s-trans*

Table 9. Computed relative energies of transition states and related stereoselectivity data for the reaction of acrolein (**18**) and TBS-protected 5-Me-silyloxyfuran (**13**).

Notation	Iminium	Attack	Product	Δ*E* [kcal mol^{-1}]	Pop [%][a]
TS-a-d/*si*	*s-trans*	d/*si*	*S*	0.16	25.7
TS-a-u/*si*	*s-trans*	u/*si*	*S*	0.25	22.0
TS-a-d/*re*	*s-trans*	d/*re*	*R*	5.06	0.0
TS-a-u/*re*	*s-trans*	u/*re*	*R*	2.34	0.6
TS-a-d/*si*′	*s-trans*′	d/*si*	*S*	0.37	18.0
TS-a-u/*si*′	*s-trans*′	u/*si*	*S*	0.00	33.6
TS-a-d/*re*′	*s-trans*′	d/*re*	*R*	4.13	0.0
TS-a-u/*re*′	*s-trans*′	u/*re*	*R*	5.12	0.0
e.r. (*S*/*R*)					99.3:0.7

[a] See footnote [b] of Table 7.

and *s-trans*′ iminium intermediates are predicted to be rather close in energy, which follows from the electrophilicities of the two iminium conformers.[15] The relative contribution of these four pathways to the formation of product isomers is 99.3 %.

Computations have also been carried out for the reactions of (*E*)-crotonaldehyde (**38**) with 5-Me- and 5*H*-silyloxyfurans. Results for the most stable transition states associated with the four product isomers are reported in Tables 10 and 11. The computed data are consistent with our experimental findings, because they show high e.r. values for both reactions and they also point to the reduction of the diastereomeric ratio (d.r.) with 5*H*-silyloxyfuran. Our analysis suggests that the diastereoselectivity of the reaction of (*E*)-crotonaldehyde (**38**) with 5-Me-silyloxyfuran **13** is related to the interaction of terminal methyl group of the iminium ion and the 5-Me substituent of the furan (see Figure 8). In the transition state leading to the major product (**TS-c5Me-d/*si***), the furan ring and the unsaturated iminium fragment display a staggered arrangement, whereas in the diastereomeric transition state (**TS-c5Me-u/*si*′**), this alignment is somewhat distorted. The closer contact of the neighboring CH_3 groups induces slight destabilization for the latter transition state. This effect is absent in transition states located for the reaction with 5*H*-silyloxyfuran **40**, therefore the diastereomeric transition states become nearly isoenergetic. This is also in excellent agreement with the experimental results (Table 6, compare entries 1 and 3).

In summary, the computational results indicate that high enantioselectivities could arise even in covalent catalysis from

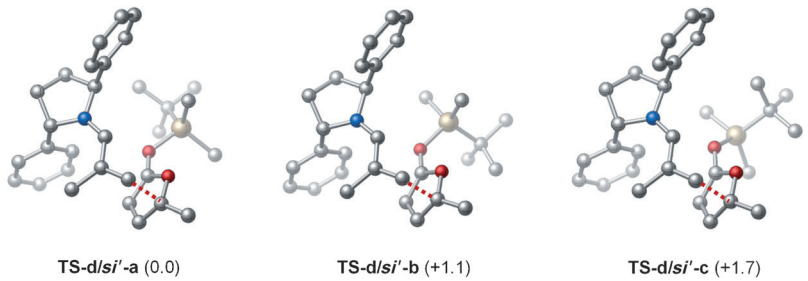

Figure 7. Relative orientation of the TBS group in transition state **TS-d/*si*′**. Relative energies are given in parenthesis (in kcal mol^{-1}). All H atoms are omitted for clarity.

Table 10. Computed relative energies of transition states and related stereoselectivity data for the reaction of acrolein (**18**) and TBS-protected 5-Me-silyloxyfuran (**13**).

Notation	Iminium	Attack	Product	ΔE [kcal mol^{-1}]	Pop [%][a]
TS-c5Me-d/*si*	*s-trans-E*	d/*si*	*R,S*	0.00	85.0
TS-c5Me-u/*si*′	*s-trans-E*′	u/*si*	*S,S*	1.03	14.9
TS-c5Me-d/*re*′	*s-trans-E*′	d/*re*	*S,R*	5.82	0.0
TS-c5Me-u/*re*′	*s-trans-E*′	u/*re*	*R,R*	3.98	0.1
(R,S)/(S,R)					99.99:0.01
(R,S)/(S,S)					85.1:14.9

[a] See footnote [b] of Table 7.

Table 11. Computed relative energies of transition states and related stereoselectivity data for the reaction of (*E*)-crotonaldehyde (**38**) and TBS-protected 5*H*-silyloxyfuran (**40**).

Notation	Iminium	Attack	Product	ΔE [kcal mol^{-1}]	Pop [%][a]
TS-c5H-d/*si*	*s-trans-E*	d/*si*	*R,S*	0.00	53.2
TS-c5H-u/*si*′	*s-trans-E*′	u/*si*	*S,S*	0.08	46.7
TS-c5H-d/*re*′	*s-trans-E*′	d/*re*	*S,R*	4.37	0.03
TS-c5H-u/*re*′	*s-trans-E*′	u/*re*	*R,R*	4.03	0.06
(R,S)/(S,R)					99.9:0.1
(R,S)/(S,S)					53.2:46.8

[a] See footnote [b] of Table 7.

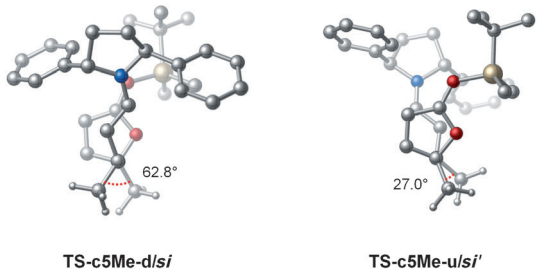

Figure 8. Diastereomeric transition states located for the reaction of (*E*)-crotonaldehyde (**38**) and TBS-protected 5-Me-silyloxyfuran (**13**). Dihedral angles characteristic of the relative orientation of the reacting species are shown for both structures. Hydrogen atoms are omitted for clarity except those of the interacting methyl groups.

a sum of attractive noncovalent interactions. Although the role of noncovalent interactions in controlling enantioselectivity has been noted before in organocatalysis[17] and metal catalysis,[24] we believe ours is the first documented example of covalent catalysis in which attractive noncovalent interactions appear to be in full control of the enantioselectivity.

Conclusion

Trans-2,5-diphenylpyrrolidine is a versatile iminium catalyst for the enantioselective Mukaiyama–Michael reaction. The high enantioselectivities obtained with this catalyst challenge the prevailing steric shielding paradigm in covalent organocatalysis. A computational analysis of the transition states suggests that the selectivity is largely due to attractive dispersion interactions, not repulsive steric shielding. We find it likely that there are many more enantioselective reactions in which the origin of enantioselectivity could be traced back to attractive van der Waals interactions instead of steric shielding, in spite of the popularity of the steric shielding models. Such considerations should be taken into account in catalyst design.

Experimental Section

General procedure for the α-substituted acroleins

α-Substituted acrolein (200–500 mol%) and silyloxyfuran (0.5 mmol mL^{-1}, 100 mol%) were added to a stirred solution of (2*S*,5*S*)-2,5-diphenylpyrrolidine (**(*S*,*S*)-12**) (20 mol%), 4-nitrobenzoic acid (20 mol%), and water (200 mol%) in CH_2Cl_2. The mixture was stirred at either 0 °C or RT. After completion of the reaction (determined by TLC, GC, or NMR spectroscopy), either the mixture was filtered through a layer of silica and concentrated, or the mixture was transferred into the flash column and purified by flash chromatography to afford the desired products.

(*S*)-3-(5-Oxo-2,5-dihydrofuran-2-yl)propanal (20): R_f (EtOAc) = 0.54; $[\alpha]_D = +60.0$ ($c = 1.1$, $CHCl_3$); ^{1}H NMR (400 MHz, $CDCl_3$): δ = 9.79 (t, 1H, J = 0.8 Hz), 7.44 (dd, 1H, J = 5.7, 1.6 Hz), 6.12 (dd, 1H, J = 5.7, 2.0 Hz), 5.11 (ddt, 1H, J = 7.9, 4.0, 2.0 Hz), 2.75–2.58 (m, 2H), 2.22 (dtd, 1H, J = 14.6, 7.3, 4.2 Hz), 1.83 ppm (dddd, 1H, J = 14.6, 8.2, 7.0, 6.2 Hz); ^{13}C NMR (100 MHz, $CDCl_3$): δ = 200.5, 172.7, 155.9, 122.0, 81.9, 38.8, 25.2 ppm; IR (film): $\tilde{\nu}$ = 2927, 2850, 1746, 1720, 1163, 1095, 817 cm^{-1}; HRMS (ESI$^+$): *m/z* calcd for [$C_7H_8O_3Na$]: 163.0371; found: 163.0363, Δ = 4.9 ppm.

(*S*)-3-(2-Methyl-5-oxo-2,5-dihydrofuran-2-yl)propanal (30): R_f (Et_2O) = 0.35; $[\alpha]_D = +39.7$ ($c = 1.0$, $CHCl_3$); ^{1}H NMR (250 MHz, $CDCl_3$): δ = 9.70 (t, 1H, J = 0.9 Hz), 7.31 (d, 1H, J = 5.6 Hz), 5.99 (d, 1H, J = 5.6 Hz), 2.50 (dddd^{AB}, 1H, J = 18.5, 8.0, 6.5, 0.9 Hz), 2.37 (dddd^{AB}, 1H, J = 18.5, 7.5, 6.7, 0.9 Hz), 2.14 (ddd^{AB}, 1H, J = 14.5, 7.5, 6.5 Hz), 2.06 (ddd^{AB}, 1H, J = 14.5, 8.0, 6.7 Hz), 1.47 ppm (s, 3H); ^{13}C NMR (63 MHz, $CDCl_3$): δ = 200.4, 172.1, 160.0, 121.0, 87.8, 38.0, 29.7, 24.3 ppm; IR (film): $\tilde{\nu}$ = 3058, 2982, 2935, 2840, 2733, 1752, 1722, 1185, 1116, 953, 822 cm^{-1}; HRMS (ESI$^+$): *m/z* calcd for [$C_8H_{10}O_3Na$]: 177.0528; found: 177.0522, Δ = 3.4 ppm.

(*S*)-3-(4-Methyl-5-oxo-2,5-dihydrofuran-2-yl)propanal (31): R_f (EtOAc) = 0.70; $[\alpha]_D = +17.7$ ($c = 1.0$, CH_2Cl_2) ^{1}H NMR (400 MHz, $CDCl_3$): δ = 9.79 (t, 1H, J = 0.8 Hz), 7.01 (qn, 1H, J = 1.6 Hz), 4.98–4.92 (m, 1H), 2.74–2.57 (m, 2H), 2.20 (dtd, 1H, J = 14.6, 7.3, 4.1 Hz), 1.91 (t, 3H, J = 1.6 Hz), 1.79 ppm (dddd, 1H, J = 14.6, 8.3, 7.3, 6.2 Hz); ^{13}C NMR (100 MHz, $CDCl_3$): δ = 200.6, 174.0, 148.2, 130.7, 79.8, 39.1, 25.6, 10.8 ppm; IR (film): $\tilde{\nu}$ = 2926, 2851, 1750, 1722, 1101, 1072, 1026, 984 cm^{-1}; HRMS (ESI$^+$): *m/z* calcd for [$C_8H_{10}O_3Na$]: 177.0528; found: 177.0526, Δ = 1.1 ppm.

(*R*)-1-Oxo-3-((*S*)-5-oxo-2,5-dihydrofuran-2-yl)propan-2-yl acetate (32a) and (*S*)-1-oxo-3-((*S*)-5-oxo-2,5-dihydrofuran-2-yl)propan-2-yl acetate (32b): R_f (Et_2O) = 0.39; ^{1}H NMR (400 MHz, $CDCl_3$, other half): δ = 9.68 (app. t, 1H, J = 0.8 Hz), 7.45 (dd, 1H, J = 5.8, 1.8 Hz), 6.12 (dd, 1H, J = 1.8, 1.2 Hz), 5.17–5.12 (m, 1H), 2.68–2.58 (m, 1H), 2.07 (ddd, 1H, J = 14.6, 8.8, 5.9 Hz), 1.80 (ddd, 1H, J = 14.6, 7.3, 4.1 Hz), 1.24 ppm (d, 3H, J = 7.4 Hz); ^{1}H NMR (400 MHz, $CDCl_3$, other half): δ = 9.64 (d, 1H, J = 0.9 Hz), 7.46 (dd, 1H, J = 5.8, 1.8 Hz), 6.10 (dd, 1H, J = 1.8, 1.2 Hz), 5.15–5.10 (m, 1H), 2.81–2.71 (m, 1H), 2.27 (ddd, 1H, J = 14.5, 8.8, 3.5 Hz), 1.44 (dddd, 1H, J = 14.5, 9.9,

4.3, 0.7 Hz), 1.22 ppm (d, 1H, $J=7.5$ Hz); ^{13}C NMR (100 MHz, $CDCl_3$, other half): $\delta=203.3$, 172.74, 156.2, 121.8, 80.9, 43.1, 34.1, 14.6 ppm; ^{13}C NMR (100 MHz, $CDCl_3$, other half): $\delta=203.1$, 172.67, 156.2, 121.9, 81.6, 42.6, 33.2, 13.6 ppm ; IR (film): $\tilde{\nu}=3092$, 2969, 2937, 2867, 2832, 2723, 1745, 1721, 1163, 1105, 1023, 910, 814 cm^{-1}; HRMS (ESI$^+$): *m/z* calcd for $[C_8H_{10}O_3Na]$: 177.0528; found: 177.0524, $\Delta=2.3$ ppm.

(*S*)-2-(((*S*)-2-Methyl-5-oxo-2,5-dihydrofuran-2-yl)methyl)pentanal (33 a): R_f (Et_2O/*n*-Pentane 2:1)=0.41; $[\alpha]_D=-53.5$ ($c=2.8$, $CHCl_3$); ^{1}H NMR (400 MHz, $CDCl_3$): $\delta=9.52$ (dd, 1H, $J=1.0$, 0.8 Hz), 7.25 (d, 1H, $J=5.6$ Hz), 5.92 (d, 1H, $J=5.6$ Hz), 2.33 (dd, 1H, $J=14.5$, 9.3 Hz), 2.24–2.15 (m, 1H), 1.83 (dd, 1H, 14.5, 1.8 Hz), 1.65–1.55 (m, 1H), 1.48 (s, 3H), 1.45–1.34 (m, 1H), 1.33 (app. sext, 2H, $J=7.3$ Hz), 0.90 ppm (t, 3H, $J=7.3$ Hz); ^{13}C NMR (100 MHz, $CDCl_3$): $\delta=203.6$, 172.3, 160.6, 120.5, 88.1, 46.3, 35.5, 32.0, 25.2, 19.9, 14.1 ppm; IR (film): $\tilde{\nu}=3085$, 2960, 2933, 2874, 2719, 1752, 1722, 1191, 1115, 952, 820 cm^{-1}; HRMS (ESI$^+$): *m/z* calcd for $[C_{11}H_{16}O_3Na]$: 219.0997; found: 219.0998, $\Delta=0.5$ ppm.

(*R*)-2-(((*S*)-2-Methyl-5-oxo-2,5-dihydrofuran-2-yl)methyl)pentanal (33 b): R_f (Et_2O/*n*-Pentane 2:1)=0.30; $[\alpha]_D=+49.4$ ($c=0.98$, $CHCl_3$); ^{1}H NMR (400 MHz, $CDCl_3$): $\delta=9.55$ (d, 1H, $J=2.7$ Hz), 7.33 (d, 1H, $J=5.6$ Hz), 6.04 (d, 1H, $J=5.6$ Hz), 2.41 (dd, 1H, $J=14.4$, 8.7 Hz), 2.38–2.29 (m, 1H), 1.67 (dd, 1H, $J=14.4$, 3.0 Hz), 1.64–1.55 (m, 1H), 1.44 (s, 3H), 1.44–1.36 (m, 1H), 1.36–1.23 (m, 2H), 0.90 ppm (t, 3H, $J=7.2$ Hz); ^{13}C NMR (100 MHz, $CDCl_3$): $\delta=203.2$, 171.9, 159.9, 121.3, 88.1, 47.3, 37.0, 32.2, 24.5, 20.0, 14.1 ppm; IR (film): $\tilde{\nu}=3085$, 2960, 2933, 2874, 2718, 1755, 1722, 1456, 1190, 1113, 952, 820 cm^{-1}; HRMS (ESI$^+$): *m/z* calcd for $[C_{11}H_{16}O_3Na]$: 219.0997; found: 219.0998, $\Delta=0.5$ ppm.

(*S*)-2-Benzyl-3-((*S*)-2-methyl-5-oxo-2,5-dihydrofuran-2-yl)propanal (34 a): R_f (Et_2O/hexanes 2:1)=0.24; $[\alpha]_D=-34.2$ ($c=1.6$, $CHCl_3$); ^{1}H NMR (400 MHz, $CDCl_3$): $\delta=9.62$ (dd, 1H, $J=1.2$, 0.8 Hz), 7.33–7.27 (m, 2H), 7.26–7.20 (m, 1H), 7.23 (d, 1H, $J=5.6$ Hz), 7.15–7.11 (m, 2H), 5.94 (d, 1H, $J=5.6$ Hz), 2.95 (dd, 1H, $J=14.0$, 7.3 Hz), 2.77 (dd, 1H, $J=14.0$, 7.3 Hz), 2.62 (app. dtdd, 1H, $J=9.2$, 7.3, 2.3, 1.2 Hz), 7.28 (dd, 1H, $J=14.7$, 9.2 Hz), 1.87 (dd, 1H, $J=14.7$, 2.3 Hz), 1.44 ppm (s, 3H); ^{13}C NMR (100 MHz, $CDCl_3$): $\delta=203.4$, 172.3, 160.7, 137.2, 129.1, 128.9, 127.1, 120.5, 88.0, 47.8, 36.4, 35.5, 25.1 ppm; IR (film): $\tilde{\nu}=3029$, 2982, 2933, 2850, 2726, 1748, 1723, 1198, 1114, 952, 819, 702 cm^{-1}; HRMS (ESI$^+$): *m/z* calcd for $[C_{15}H_{16}O_3Na]$: 267.0997; found: 267.1002, $\Delta=1.9$ ppm.

(*R*)-2-Benzyl-3-((*S*)-2-methyl-5-oxo-2,5-dihydrofuran-2-yl)propanal (34 b): R_f (Et_2O/hexanes 2:1)=0.17; $[\alpha]_D=+69.4$ ($c=0.6$, 89:11 mixture of **34 b**/**34 a**, $CHCl_3$); ^{1}H NMR (400 MHz, $CDCl_3$): $\delta=9.65$ (d, 1H, $J=2.3$ Hz), 7.33–7.20 (m, 3H), 7.15–7.09 (m, 2H), 7.05 (d, 1H, $J=5.6$ Hz), 6.00 (d, 1H, $J=5.6$ Hz), 2.96 (dd, 1H, $J=13.8$, 6.5 Hz), 2.67 (dd, 1H, $J=13.8$, 8.3 Hz), 2.57 (tddd, 1H, $J=8.3$, 6.5, 3.1, 2.3 Hz), 2.42 (dd, 1H, $J=14.8$, 8.3 Hz), 1.68 (dd, 1H, $J=14.8$, 3.1 Hz), 1.40 ppm (s, 3H); ^{13}C NMR (100 MHz, $CDCl_3$): $\delta=202.6$, 171.8, 160.0, 137.5, 129.2, 128.9, 127.0, 121.4, 87.9, 48.7, 36.1, 36.0, 24.7 ppm; IR (film): $\tilde{\nu}=3030$, 2982, 2930, 2851, 1754, 1724, 1455, 1114, 951, 819, 702 cm^{-1}; HRMS (ESI$^+$): *m/z* calcd for $[C_{15}H_{16}O_3Na]$: 267.0997; found: 267.1003, $\Delta=2.2$ ppm.

(*S*)-1-Oxo-3-((*S*)-5-oxo-2,5-dihydrofuran-2-yl)propan-2-yl acetate (35 a) and (*R*)-1-oxo-3-((*S*)-5-oxo-2,5-dihydrofuran-2-yl)propan-2-yl acetate (35 b): R_f (Et_2O)=0.09; ^{1}H NMR (400 MHz, $CDCl_3$, major): $\delta=9.57$ (s, 1H), 7.48 (dd, 1H, $J=5.7$, 1.5 Hz), 6.15 (dd, 1H, $J=5.7$, 2.0 Hz), 5.25–5.15 (m, 2H), 2.42 (ddd, 1H, $J=15.0$, 4.9 Hz), 2.20 (s, 3H), 2.20–2.08 ppm (m, 1H); ^{1}H NMR (400 MHz, $CDCl_3$, minor): $\delta=9.55$ (s, 1H), 7.47 (dd, 1H, $J=5.7$, 1.6 Hz), 6.18 (dd, 1H, $J=5.7$, 2.0 Hz), 5.25–5.15 (m, 2H), 2.21 (s, 3H), 2.27–2.08 ppm (m, 2H); ^{13}C NMR (100 MHz, $CDCl_3$, major): $\delta=197.4$, 172.0, 170.2, 155.1, 122.3, 79.3, 74.5, 32.8, 20.7 ppm; ^{13}C NMR (100 MHz, $CDCl_3$, minor): $\delta=196.9$, 172.1, 170.2, 155.2, 122.6, 79.0, 75.1, 32.4, 20.6 ppm; IR (film): $\tilde{\nu}=3469$, 3101, 2926, 2850, 1736, 1373, 1231, 1164, 1100 cm^{-1}; HRMS (ESI$^+$): *m/z* calcd for $[C_7H_{10}O_5Na]$: 221.0426; found: 221.0424, $\Delta=0.9$ ppm.

(*S*)-1-((*S*)-2-Methyl-5-oxo-2,5-dihydrofuran-2-yl)-3-oxopropan-2-yl acetate (36 a) and (*R*)-1-((*S*)-2-methyl-5-oxo-2,5-dihydrofuran-2-yl)-3-oxopropan-2-yl acetate (36 b): R_f (Et_2O)=0.13; ^{1}H NMR (400 MHz, $CDCl_3$, other half): $\delta=9.46$ (s, 1H), 7.36 (d, 1H, $J=5.6$ Hz), 5.99 (d, 1H, $J=5.6$ Hz), 4.98 (dd, 1H, $J=9.0$, 2.9 Hz), 2.52 (dd, 1H, $J=15.4$, 2.9 Hz), 2.13 (dd, 1H, $J=15.4$, 9.0 Hz), 2.12 (s, 3H), 1.51 ppm (s, 3H); ^{1}H NMR (400 MHz, $CDCl_3$, other half): $\delta=9.45$ (s, 1H), 7.39 (d, 1H, $J=5.6$ Hz), 6.05 (d, 1H, $J=5.6$ Hz), 4.94 (dd, 1H, $J=8.0$, 4.2 Hz), 2.35 (dd, 1H, $J=15.4$, 4.2 Hz), 2.28 (dd, 1H, $J=15.4$, 8.0 Hz), 2.15 (s, 3H), 1.50 ppm (s, 3H); ^{13}C NMR (100 MHz, $CDCl_3$, other half): $\delta=197.1$, 171.7, 170.3, 159.6, 121.5, 86.2, 74.1, 36.6, 25.1, 20.6 ppm; ^{13}C NMR (100 MHz, $CDCl_3$, other half): $\delta=197.1$, 171.6, 169.9, 159.2, 120.5, 86.7, 75.1, 36.5, 24.7, 20.6 ppm; IR (film): $\tilde{\nu}=3467$, 2982, 2937, 2842, 1742, 1373, 1229, 1123, 956, 825 cm^{-1}; HRMS (ESI$^+$): *m/z* calcd for $[C_{10}H_{12}O_5Na]$: 235.0582; found: 235.0584, $\Delta=0.9$ ppm.

(*S*)-2-(Benzyloxy)-3-((*S*)-2-methyl-5-oxo-2,5-dihydrofuran-2-yl)-propanal (37 a) and (*R*)-2-(benzyloxy)-3-((*S*)-2-methyl-5-oxo-2,5-dihydrofuran-2-yl)propanal (37 b): Major diastereomer: R_f (1:1 EtOAc/hexanes)=0.53; $[\alpha]_D=+44.7$ ($c=0.7$, CH_2Cl_2); ^{1}H NMR (400 MHz, $CDCl_3$): $\delta=9.61$ (d, 1H, $J=1.1$ Hz), 7.41 (d, 1H, $J=5.6$ Hz), 7.40–7.28 (m, 5H), 5.90 (d, 1H, $J=5.6$ Hz), 4.55 (d, 1H, $J=11.0$ Hz), 4.32 (d, 1H, $J=11.0$ Hz), 3.68 (ddd, 1H, $J=9.5$, 2.4, 1.1 Hz), 2.38 (dd, 1H, $J=15.1$, 2.4 Hz), 2.06 (dd, 1H, $J=15.1$, 9.5 Hz), 1.51 ppm (s, 3H); ^{13}C NMR (100 MHz, $CDCl_3$): $\delta=201.3$, 172.4, 161.1, 136.6, 128.8, 128.51, 128.46, 118.8, 86.6, 79.7, 73.0, 38.7, 25.6 ppm; IR (film): $\tilde{\nu}=3430$, 2981, 2931, 2873, 2854, 1729, 1454, 1115, 953, 820, 739 cm^{-1}; HRMS (ESI$^+$): *m/z* calcd for $[C_{15}H_{16}O_4Na]$: 283.0946; found: 283.0951, $\Delta=1.8$ ppm. Minor diastereomer: R_f (1:1 EtOAc/hexanes)=0.43; $[\alpha]_D=-4.1$ ($c=1.3$, 23:77 mixture of the major and minor diastereomers, CH_2Cl_2); ^{1}H NMR (400 MHz, $CDCl_3$): $\delta=9.62$ (d, 1H, $J=1.4$ Hz), 7.43 (d, 1H, $J=5.7$ Hz), 7.40–7.28 (m, 5H), 5.97 (d, 1H, $J=5.7$ Hz), 4.68 (d, 1H, $J=11.4$ Hz), 4.56 (d, 1H, $J=11.4$ Hz), 3.87 (ddd, 1H, $J=7.8$, 4.3, 1.4 Hz), 2.18 (dd, 1H, $J=14.8$, 4.3 Hz), 2.10 (dd, 1H, $J=14.7$, 7.8 Hz), 1.47 ppm (s, 3H); ^{13}C NMR (100 MHz, $CDCl_3$): $\delta=201.6$, 172.0, 160.7, 136.6, 128.9, 128.6, 128.5, 120.2, 87.1, 80.1, 73.0, 38.5, 24.1 ppm; IR (film): $\tilde{\nu}=3410$, 2982, 2933, 2875, 1753, 1115, 953, 821 cm^{-1}; HRMS (ESI$^+$): *m/z* calcd for $[C_{15}H_{16}O_4Na]$: 283.0946; found: 283.0952, $\Delta=2.1$ ppm.

General procedure for the β-substituted acroleins

$KHSO_4$ solution (sat. aq. containing $KHSO_4$ (58 mol%) and water (840 mol%) was added to a stirred solution of (2*S*,5*S*)-2,5-diphenylpyrrolidine ((*S*,*S*)-**12**) (20 mol%) and 4-nitrobenzoic acid (20 mol%) in CH_2Cl_2 at RT, and the reaction mixture was cooled to 0 °C. β-Substituted acrolein (500–1000 mol%) was added to the reaction mixture and it was stirred at 0 °C for 10 min, after which the silyloxyfuran (0.25 mmol mL^{-1}, 100 mol%) was added and the reaction mixture was stirred at 0 °C for the given time. After completion of the reaction (determined by TLC), the mixture was transferred into the flash column and purified by flash chromatography to afford the desired products.

(*R*)-3-((*S*)-2-Methyl-5-oxo-2,5-dihydrofuran-2-yl)butanal (41 a) and (*S*)-3-((*S*)-2-methyl-5-oxo-2,5-dihydrofuran-2-yl)butanal (41 b): R_f (EtOAc/hexanes 1:1)=0.46; $[\alpha]_D=+48.6$ ($c=1.4$, $CHCl_3$); ^{1}H NMR (250 MHz, $CDCl_3$, major (*R*,*S*)-diastereomer): $\delta=9.73$ (dd, 1H, $J=1.9$, 0.9 Hz), 7.37 (d, 1H, $J=5.7$ Hz), 6.08 (d, 1H, $J=5.7$ Hz), 2.64–2.50 (m, 2H), 2.29–2.16 (m, 1H), 1.47 (s, 3H), 0.99 ppm (d, 3H,

$J=6.7$ Hz); ^{1}H NMR (250 MHz, $CDCl_3$, minor (*S*,*S*)-diastereomer): $\delta=$ 9.71 (dd, 1H, $J=1.7$, 0.9 Hz), 7.39 (d, 1H, $J=5.7$ Hz), 6.03 (d, 1H, $J=5.7$ Hz), 2.64–2.50 (m, 2H), 2.29–2.16 (m, 1H), 1.43 (s, 3H), 1.08 ppm (d, 3H, $J=6.7$ Hz); ^{13}C NMR (100 MHz, $CDCl_3$, major (*R*,*S*)-diastereomer): $\delta=200.5$, 172.1, 158.8, 121.6, 90.5, 45.7, 34.8, 22.8, 15.8 ppm; ^{13}C NMR (100 MHz, $CDCl_3$, minor (*S*,*S*)-diastereomer): $\delta=$ 200.5, 172.1, 160.1, 122.1, 90.4, 46.1, 34.7, 20.7, 15.6 ppm; IR (film): $\tilde{\nu}=2978$, 1748, 1386, 1242, 1110, 953, 824, 781 cm^{-1}; HRMS (ESI$^+$): *m/z* calcd for [$C_9H_{12}O_3Na$]: 191.0684; found: 191.0687, $\Delta=1.6$ ppm.

(*R*)-3-((*S*)-5-Oxo-2,5-dihydrofuran-2-yl)butanal (42a) and (*S*)-3-((*S*)-5-oxo-2,5-dihydrofuran-2-yl)butanal (42b): R_f (EtOAc/hexanes 1:1) = 0.32; ^{1}H NMR (250 MHz, $CDCl_3$, major (*S*,*S*)-diastereomer): $\delta=$ 9.77 (br s, 1H), 7.41 (dd, 1H, $J=5.8$, 1.2 Hz), 6.15 (dd, 1H, $J=5.8$, 1.9 Hz), 5.11–5.08 (m, 1H), 2.76–2.33 (m, 3H), 0.87 ppm (d, 3H, $J=$ 6.6 Hz); ^{1}H NMR (250 MHz, $CDCl_3$, minor (*R*,*S*)-diastereomer): $\delta=$ 9.72 (br s, 1H), 7.45 (dd, 1H, $J=5.8$, 1.2 Hz), 6.13 (dd, 1H, $J=5.8$, 1.9 Hz), 4.95–4.89 (m, 1H), 2.76–2.33 (m, 3H), 1.11 ppm (d, 3H, $J=$ 6.6 Hz); ^{13}C NMR (63 MHz, $CDCl_3$, major (*R*,*S*)-diastereomer): $\delta=$ 200.6, 172.9, 154.8, 122.7, 86.3, 46.8, 30.0, 13.7 ppm; ^{13}C NMR (63 MHz, $CDCl_3$, minor (*S*,*S*)-diastereomer): $\delta=200.4$, 172.7, 154.9, 122.5, 85.2, 45.6, 31.2, 16.8 ppm; IR (film): $\tilde{\nu}=2968$, 2925, 1745, 1600, 1459, 1384, 1298, 1166, 1096, 1017, 897, 820, 794, 706 cm^{-1}; HRMS (ESI$^+$): *m/z* calcd for [$C_8H_{10}O_3Na$]: 177.0528; found: 177.0525, $\Delta=1.7$ ppm.

(*R*)-3-((*S*)-2-Methyl-5-oxo-2,5-dihydrofuran-2-yl)hexanal (43a) and (*S*)-3-((*S*)-2-methyl-5-oxo-2,5-dihydrofuran-2-yl)hexanal (43b): R_f (EtOAc/hexanes 1:1) = 0.43; $[\alpha]_D=+27.5$ ($c=1.06$, $CHCl_3$); ^{1}H NMR (250 MHz, $CDCl_3$, major diastereomer): $\delta=9.75$ (br s, 1H), 7.35 (d, 1H, $J=5.6$ Hz), 6.07 (d, 1H, $J=5.6$ Hz), 2.52–2.29 (m, 3H), 1.47 (s, 3H), 1.39–1.15 (m, 4H), 0.89 ppm (t, 3H, $J=7.0$ Hz); ^{1}H NMR (400 MHz, $CDCl_3$, minor diastereomer): $\delta=9.72$ (s, 1H), 7.39 (d, 1H, $J=5.6$ Hz), 6.01 (d, 1H, $J=5.6$ Hz), 2.52–2.29 (m, 3H), 1.44 (s, 3H), 1.39–1.15 (m, 4H), 0.89 ppm (t, 3H, $J=7.0$ Hz); ^{13}C NMR (100 MHz, $CDCl_3$, major diastereomer): $\delta=200.7$, 172.0, 159.1, 121.7, 90.9, 44.2, 39.9, 33.0, 23.2, 21.1, 14.2 ppm; ^{13}C NMR (100 MHz, $CDCl_3$, minor diastereomer): $\delta=200.8$, 172.2, 160.5, 120.8, 90.7, 44.5, 39.2, 32.6, 21.3, 21.0, 14.2 ppm; IR (film): $\tilde{\nu}=2960$, 2934, 2873, 1750, 1723, 1603, 1458, 1382, 1243, 1117, 1038, 952, 823, 694 cm^{-1}; HRMS (ESI$^+$): *m/z* calcd for [$C_{11}H_{16}O_3Na$]: 219.0997; found: 219.0999, $\Delta=0.9$ ppm.

(*R*)-3-((*S*)-5-Oxo-2,5-dihydrofuran-2-yl)hexanal (44a) and (*S*)-3-((*S*)-5-oxo-2,5-dihydrofuran-2-yl)hexanal (44b): R_f (EtOAc/hexanes 1:1) = 0.51; ^{1}H NMR (400 MHz, $CDCl_3$, major diastereomer): $\delta=9.71$ (t, 1H, $J=1.2$ Hz), 7.40 (dd, 1H, $J=5.8$, 1.5 Hz), 6.11 (dd, 1H, $J=5.8$, 2.2 Hz), 5.11 (dt, 1H, $J=3.8$, 1.8 Hz), 2.61–2.38 (m, 3H), 1.59–1.48 (m, 1H), 1.43–1.35 (m, 2H), 1.31–1.22 (m, 1H), 0.92 ppm (t, 3H, $J=$ 7.0 Hz); ^{1}H NMR (400 MHz, $CDCl_3$, minor diastereomer): $\delta=9.77$ (t, 1H, $J=1.2$ Hz), 7.43 (dd, 1H, $J=5.8$, 1.5 Hz), 6.16 (dd, 1H, $J=5.8$, 2.2 Hz), 5.15 (dt, 1H, $J=3.8$, 1.8 Hz), 2.61–2.38 (m, 3H), 1.59–1.48 (m, 1H), 1.43–1.35 (m, 2H), 1.31–1.22 (m, 1H), 0.88 ppm (t, 3H, $J=$ 7.0 Hz); ^{13}C NMR (100 MHz, $CDCl_3$, major diastereomer): $\delta=200.6$, 172.8, 155.7, 122.3, 84.7, 43.1, 35.1, 33.9, 20.5, 14.1 ppm; ^{13}C NMR (100 MHz, $CDCl_3$, minor diastereomer): $\delta=200.8$, 172.8, 154.6, 122.9, 84.9, 44.4, 35.0, 31.1, 20.5, 14.1 ppm; IR (film): $\tilde{\nu}=2960$, 2932, 2874, 2731, 1749, 1720, 1600, 1466, 1382, 1316, 1163, 1098, 1024, 900, 820, 794, 704 cm^{-1}; HRMS (ESI$^+$): *m/z* calcd for [$C_{10}H_{14}O_3Na$]: 205.0845; found: 205.0841, $\Delta=2.0$ ppm.

Computational approach

In the present study, the geometries of the stationary points were optimized by using density functional theory (DFT) at the ωB97X-D/6–311G(d,p) level. Herein, ωB97X-D denotes the long-range corrected hybrid density functional with damped atom-atom dispersion corrections developed by Chai and Head-Gordon.[25,26] This functional was found to be a very promising DFT method[27] yielding reasonably accurate data for general main group thermochemistry, kinetics, and noncovalent interactions (all relevant to our present work). Normal coordinate analysis was carried out at the same level of theory for all optimized structures. The results were utilized to verify the nature of the stationary points (i.e., minima or transition states), and to estimate the zero-point energies as well as the thermal and entropic contributions to the Gibbs free energies. For each located structure, additional single-point energy calculations were performed at the ωB97X-D/6–311++G(3df,3pd) level to increase the accuracy of electronic structure predictions. In all DFT calculations, the ultra-fine integration grid was employed as implemented in the Gaussian 09 package.[28]

The stereoselectivity data (i.e., enantiomeric and diastereomeric ratios) were obtained from the relative energies of stereoisomeric transition states by applying the Boltzmann distribution formula. Conceptually, solvent-phase Gibbs free energies should be appropriate for this purpose. However, considering the empirical ingredients of the polarizable continuum solvent models used to estimate the solvent effects, and the approximations employed in the calculation of entropic contributions, the error bar on the relative Gibbs free energies is expected to be significantly larger than that of the electronic energy predictions. For this reason, the relative energies and stereoselectivity data reported throughout this paper are those obtained from gas-phase ωB97X-D/6–3111++G(3df,3pd)//ωB97X-D/6–311G(d,p) electronic energies. In the present approach we thus assume that both entropic and solvent effects are similar for the stereoisomeric transition states. Our test calculations provide support for this approach (see Section 9.5. in the Supporting Information). In these computations, the thermochemical data were obtained within the ideal gas rigid-rotor harmonic oscillator approximation for $T=298.15$ K and $c=1$ mol dm^{-3} conditions. The solvation free-energies (solvent = CH_2Cl_2) were estimated at the ωB97X-D/6–311G(d,p) level by using the integral equation formalism variant of the polarizable continuum model (IEFPCM).[29] The atomic radii and non-electrostatic terms in the IEFPCM calculations were those introduced recently by Truhlar and co-workers (SMD solvation model).[30]

Acknowledgements

This work was supported by the Academy of Finland (project Nos. 138854 and 139046), by the Hungarian Research Foundation (OTKA, Grant NN-82955) and COST CM0905. We thank Dr. Elina Kalenius and Ms. Mirja Lahtiperä for assistance with mass spectrometry and Mr. Esa Haapaniemi for NMR assistance.

Keywords: DFT calculations · enantioselectivity · noncovalent interactions · organocatalysis · transition states

[1] P. J. Walsh, M. C. Kozlowski, *Fundamentals of Asymmetric Catalysis*, University Science Books, Sausalito, California, **2009**; see the discussion on pp. 115–116.
[2] H. C. Kolb, M. S. VanNieuwenhze, K. B. Sharpless, *Chem. Rev.* **1994**, *94*, 2483–2547.
[3] a) A. Erkkilä, I. Majander, P. M. Pihko, *Chem. Rev.* **2007**, *107*, 5416; b) P. M. Pihko, I. Majander, A. Erkkilä, *Top. Curr. Chem.* **2009**, *291*, 29–75.
[4] For examples, see the quadrant models discussed in Ref. [1], Chapter 4.
[5] K. C. Harper, M. S. Sigman, *J. Org. Chem.* **2013**, *78*, 2813–2818.

[6] a) Isolation and characterization: T. Yasumoto, M. Murata, Y. Oshima, M. Sano, G. K. Matsumoto, J. Clardy, *Tetrahedron* **1985**, *41*, 1019–1025; b) K. Sasaki, J. L. C. Wright, T. Yasumoto, *J. Org. Chem.* **1998**, *63*, 2475. For the total synthesis of PTX4 and PTX8, see: c) D. A. Evans, H. A. Rajapakse, D. Stenkamp, *Angew. Chem.* **2002**, *114*, 4751; *Angew. Chem. Int. Ed.* **2002**, *41*, 4569; d) D. A. Evans, H. A. Rajapakse, A. Chiu, D. Stenkamp, *Angew. Chem.* **2002**, *114*, 4755; *Angew. Chem. Int. Ed.* **2002**, *41*, 4573. For a recent total synthesis of pectenotoxin-2, see: e) K. Fujiwara, Y. Suzuki, N. Koseki, Y.-i. Aki, Y. Kikuchi, S.-i. Murata, F. Yamamoto, M. Kawamura, T. Norikura, H. Matsue, A. Murai, R. Katoono, H. Kawai, T. Suzuki, *Angew. Chem. Int. Ed.* **2014**, *53*, 780. For a review covering all synthetic studies towards the pectenotoxins until the year 2006, see: f) R. Halim, M. A. Brimble, *Org. Biomol. Chem.* **2006**, *4*, 4048–4058. For synthetic studies published after this review, see: g) K. Fujiwara, Y. Aki, F. Yamamoto, M. Kawamura, M. Kobayashi, A. Okano, D. Awakura, S. Shiga, A. Murai, H. Kawai, T. Suzuki, *Tetrahedron Lett.* **2007**, *48*, 4523; h) R. V. Kolakowski, L. J. Williams, *Tetrahedron Lett.* **2007**, *48*, 4761; i) P. D. O'Connor, C. K. Knight, D. Friedrich, X. Peng, L. A. Paquette, *J. Org. Chem.* **2007**, *72*, 1747; j) D. Vellucci, S. D. Rychnovsky, *Org. Lett.* **2007**, *9*, 711; k) S. D. Lotesta, Y. Hou, L. J. Williams, *Org. Lett.* **2007**, *9*, 869; l) A. M. Heapy, T. W. Wagner, M. A. Brimble, *Synlett* **2007**, 2359; m) S. Carley, M. A. Brimble, *Org. Lett.* **2009**, *11*, 563; n) A. M. Heapy, M. A. Brimble, *Tetrahedron* **2010**, *66*, 5424; o) S. Joyasawal, S. D. Lotesta, N. G. Akhmedov, L. J. Williams, *Org. Lett.* **2010**, *12*, 988; p) G. Vassilikogiannakis, I. Alexopoulou, M. Tofi, T. Montagnon, *Chem. Commun.* **2011**, *47*, 259–261; q) D. P. Canterbury, G. C. Micalizio, *Org. Lett.* **2011**, *13*, 2384–2387; r) K. Fujiwara, Y. Suzuki, N. Koseki, S.-I. Murata, A. Murai, H. Kawai, T. Suzuki, *Tetrahedron Lett.* **2011**, *52*, 5589–5592; s) A. Kouridaki, T. Montagnon, M. Tofi, G. Vassilikogiannakis, *Org. Lett.* **2012**, *14*, 2374–2377; t) O. Kubo, D. P. Canterbury, G. C. Micalizio, *Org. Lett.* **2012**, *14*, 5748–5751; u) A. Kouridaki, T. Montagnon, D. Kalaitzakis, G. Vassilikogiannakis, *Org. Biomol. Chem.* **2013**, *11*, 537–541; v) T. J. Donohoe, R. M. Lipinski, *Angew. Chem. Int. Ed.* **2013**, *52*, 2491–2494.

[7] a) E. K. Kemppainen, G. Sahoo, A. Valkonen, P. M. Pihko, *Org. Lett.* **2012**, *14*, 1086–1089. For previous work from this laboratory, see: b) P. M. Pihko, J. E. Aho, *Org. Lett.* **2004**, *6*, 3849–3852; c) J. E. Aho, E. Salomäki, K. Rissanen, P. M. Pihko, *Org. Lett.* **2008**, *10*, 4179–4182; d) H. Helmboldt, J. E. Aho, P. M. Pihko, *Org. Lett.* **2008**, *10*, 4183–4185; e) J. E. Aho, A. Piisola, K. S. Krishnan, P. M. Pihko, *Eur. J. Org. Chem.* **2011**, 1682.

[8] Examples of iminium-catalyzed reactions with α-substituted acroleins in which the products are cyclized during the reaction: Epoxidations: a) A. Erkkilä, P. M. Pihko, M.-R. Clarke, *Adv. Synth. Catal.* **2007**, *349*, 802–806; b) O. Lifchits, C. M. Reisinger, B. List, *J. Am. Chem. Soc.* **2010**, *132*, 10227–10229; Cyclopropanations: c) V. Terrasson, A. van der Lee, R. M. de Figueiredo, J. M. Campagne, *Chem. Eur. J.* **2010**, *16*, 7875–7880; Cycloadditions: d) K. Ishihara, K. Nakano, *J. Am. Chem. Soc.* **2005**, *127*, 10504–10505; e) A. Sakakura, K. Suzuki, K. Nakano, K. Ishihara, *Org. Lett.* **2006**, *8*, 2229–2232; f) A. Sakakura, K. Suzuki, K. Ishihara, *Adv. Synth. Catal.* **2006**, *348*, 2457–2465; g) K. Ishihara, K. Nakano, M. Akakura, *Org. Lett.* **2008**, *10*, 2893–2896; h) K. Ishihara, K. Nakano, *J. Am. Chem. Soc.* **2007**, *129*, 8930–8931; i) T. Kano, Y. Tanaka, K. Osawa, T. Yurino, K. Maruoka, *Chem. Commun.* **2009**, *15*, 1956–1958; Aziridinations: j) L. Deiana, P. Dziedzic, G.-L Zhao, J. Vesely, I. Ibrahem, R. Rios, J. Sun, A. Córdova, *Chem. Eur. J.* **2011**, *17*, 7904–7917.

[9] N. Halland, A. Braunton, S. Bachmann, M. Marigo, K. A. Jørgensen, *J. Am. Chem. Soc.* **2004**, *126*, 4790–4791.

[10] S. P. Brown, N. C. Goodwin, D. W. C. MacMillan, *J. Am. Chem. Soc.* **2003**, *125*, 1192–1194.

[11] a) Y. Hayashi, H. Gotoh, T. Hayashi, M. Shoji, *Angew. Chem.* **2005**, *117*, 4284–4287; *Angew. Chem. Int. Ed.* **2005**, *44*, 4212–4215; b) M. Marigo, T. C. Wabnitz, D. Fielenbach, K. A. Jørgensen, *Angew. Chem.* **2005**, *117*, 804–807; *Angew. Chem. Int. Ed.* **2005**, *44*, 794–797.

[12] M. Benohoud, A. Erkkilä, P. M. Pihko, *Org. Synth.* **2010**, *87*, 201–208.

[13] For details, see the Experimental Section: "Computational approach".

[14] Correlation between electrophilicity and the distortion of the iminium unit is analyzed in the Supporting Information.

[15] For details, see the Supporting Information.

[16] The preference of "closed" transition structures in the C–C bond formation between the iminium ion and pyrrole has been noted previously, and it has been associated with electrostatic stabilization of the developing partial charge on the pyrrole by the iminium π-system. See: R. Gordillo, J. Carter, K. N. Houk, *Adv. Synth. Catal.* **2004**, *346*, 1175.

[17] For the importance of stabilizing secondary interactions in organocatalytic reactions, see: a) P. H. Cheong, C. Y. Legault, J. M. Um, N. Çelebi-Ölçüm, K. N. Houk, *Chem. Rev.* **2011**, *111*, 5042; b) I. Pápai in *Science of Synthesis: Asymmetric Organocatalysis, Vol. 2* (Eds.: B. List, K. Maruoka), Thieme, Stuttgart, **2012**, pp. 601–632.

[18] For the effect of weak stabilizing interactions in iminium intermediates, see: a) J. B. Brazier, G. Evans, T. J. K. Gibbs, S. J. Coles, M. B. Hursthouse, J. A. Platts, N. C. O. Tomkinson, *Org. Lett.* **2009**, *11*, 133; b) R. Gordillo, K. N. Houk, *J. Am. Chem. Soc.* **2006**, *128*, 3543.

[19] The RDG data were computed by using the NCIPLOT program. For basic reference, see: a) E. R. Johnson, S. Keinan, P. Mori-Sánchez, J. Contreras-García, A. J. Cohen, W. Yang, *J. Am. Chem. Soc.* **2010**, *132*, 6498; b) J. Contreras-García, E. R. Johnson, S. Keinan, R. Chaudret, J. Piquemal, D. N. Beratan, W. Yang, *J. Chem. Theory Comput.* **2011**, *7*, 625.

[20] RDG isosurface plots were visualized by the VMD program: W. Humphrey, A. Dalke, K. Schulten, *J. Molec. Graphics* **1996**, *14*, 33.

[21] The truncated models were derived from the original transition states keeping all structural parameters. The H atoms of the SiH_3 and SiH units were aligned with the corresponding bonds with Si–H bond distances of 1.48 Å (computed equilibrium bond length of SiH_4). The reported relative energies were obtained from single-point ωB97X-D/6–311G(d,p) calculations.

[22] Both carbon atoms involved in C–C bond formation are pyramidalized in the transition state, that is, distorted from their equilibrium structures.

[23] A very similar trend in interaction energies was obtained with a smaller model involving a benzene molecule interacting with a silyloxyfuran. These results suggest that energy differences obtained by *model-1* are due to differential *fur···Ph* interactions. For further details regarding the model systems, see the Supporting Information.

[24] Recently, attractive noncovalent interactions were invoked as the source of enantioselectivity in a silver-catalyzed reaction. However, this reaction proceeds with relatively low selectivity (73% *ee*, corresponding to only 0.7 kcal mol^{-1} difference in the transition states). See: J. L. Arbour, H. S. Rzepa, J. Contreras-Garcia, L. A. Adrio, E. M. Barreiro, K. K. M. Hii, *Chem. Eur. J.* **2012**, *18*, 11317.

[25] For the ωB97X-D functional, see: a) J.-D. Chai, M. Head-Gordon, *Phys. Chem. Chem. Phys.* **2008**, *10*, 6615; b) J.-D. Chai, M. Head-Gordon, *J. Chem. Phys.* **2008**, *128*, 084106.

[26] For the 6–311G(d,p) and 6–311++G(3df,3pd) basis sets, see: a) R. Krishnan, J. S. Binkley, R. Seeger, J. A. Pople, *J. Chem. Phys.* **1980**, *72*, 650; b) A. D. McLean, G. S. Chandler, *J. Chem. Phys.* **1980**, *72*, 5639; c) T. Clark, J. Chandrasekhar, G. W. Spitznagel, P. v. R. Schleyer, *J. Comput. Chem.* **1983**, *4*, 294; d) M. J. Frisch, J. A. Pople, J. S. Binkley, *J. Chem. Phys.* **1984**, *80*, 3265.

[27] L. Goerigk, S. Grimme, *Phys. Chem. Chem. Phys.* **2011**, *13*, 6670.

[28] Gaussian 09, Revision A.02, M. J. Frisch, G. W. Trucks, H. B. Schlegel, G. E. Scuseria, M. A. Robb, J. R. Cheeseman, G. Scalmani, V. Barone, B. Mennucci, G. A. Petersson, H. Nakatsuji, M. Caricato, X. Li, H. P. Hratchian, A. F. Izmaylov, J. Bloino, G. Zheng, J. L. Sonnenberg, M. Hada, M. Ehara, K. Toyota, R. Fukuda, J. Hasegawa, M. Ishida, T. Nakajima, Y. Honda, O. Kitao, H. Nakai, T. Vreven, J. A. Montgomery, J. E. Peralta, F. Ogliaro, M. Bearpark, J. J. Heyd, E. Brothers, K. N. Kudin, V. N. Staroverov, R. Kobayashi, J. Normand, K. Raghavachari, A. Rendell, J. C. Burant, S. S. Iyengar, J. Tomasi, M. Cossi, N. Rega, J. M. Millam, M. Klene, J. E. Knox, J. B. Cross, V. Bakken, C. Adamo, J. Jaramillo, R. Gomperts, R. E. Stratmann, O. Yazyev, A. J. Austin, R. Cammi, C. Pomelli, J. W. Ochterski, R. L. Martin, K. Morokuma, V. G. Zakrzewski, G. A. Voth, P. Salvador, J. J. Dannenberg, S. Dapprich, A. D. Daniels, O. Farkas, J. B. Foresman, J. V. Ortiz, J. Cioslowski, D. J. Fox, Gaussian, Inc., Wallingford CT, **2009**.

[29] J. Tomasi, B. Mennucci, E. Cancès, *J. Mol. Struct.* **1999**, *464*, 211.

[30] A. V. Marenich, C. J. Cramer, D. G. Truhlar, *J. Phys. Chem. B* **2009**, *113*, 6378.

Received: October 30, 2013
Published online on ■■ ▮▮, 2014

FULL PAPER

Enantioselectivity

E. K. Kemppainen, G. Sahoo, A. Piisola, A. Hamza, B. Kótai, I. Pápai, P. M. Pihko**

■■ – ■■

Mukaiyama–Michael Reactions with *Trans*-2,5-Diarylpyrrolidine Catalysts: Enantioselectivity Arises from Attractive Noncovalent Interactions, Not from Steric Hindrance

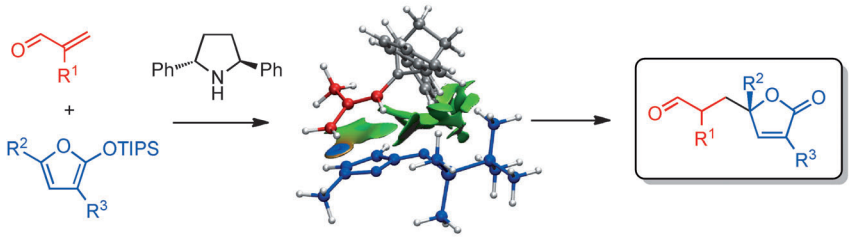

attractive noncovalent interactions *induce stereoselectivity*

Embraced enantioselectivity: Mukaiyama–Michael reactions catalyzed by *trans*-2,5-diphenylpyrrolidine catalyst are highly enantioselective, but why? The answer appears to lie in the attractive, not repulsive, noncovalent interactions in the transition states leading to the major product(s) (see scheme; TIPS = triisopropylsilyl).